A Study of the Supramolecular Approach in Controlling Diblock Copolymer Nanopatterning and Nanoporosity on Surfaces

Alexis Laforgue,† C. Geraldine Bazuin,* and Robert E. Prud'homme*

Département de chimie, Université de Montréal, C.P. 6128 Succ. Centre-Ville, Montréal (QC), Canada H3C 3J7

Received May 19, 2006; Revised Manuscript Received July 17, 2006

ABSTRACT: Thin films of poly(styrene-*b*-4-vinylpyridine) (PS4VP) [M_n(PS) = 71.9 kg/mol; M_n(P4VP) = 30.2 kg/mol] mixed with 1,5-dihydroxynaphthalene (DHN) were dip-coated onto flat substrates from THF solutions. The resultant nanostructures were characterized by AFM, TEM, infrared spectroscopy, contact angle measurements, and cyclic voltammetry. The DHN selectively enriches the P4VP domains through hydrogen bond complexation, giving relative block compositions that should result in lamellar morphology in the bulk. However, films dip-coated from solutions of variable DHN:4VP molar ratios self-assemble into a quasi-hexagonal array of nodules of P4VP + DHN protruding above a PS matrix. This morphology can be ascribed, at least in part, to greater solubility in THF of PS compared to P4VP. The solubility difference appears to be highest for equimolar DHN:4VP. The removal of DHN from the deposited films by rinsing with methanol creates regularly patterned nanoporous films. The geometric parameters of the nanopatterns before and after DHN removal depend on the DHN:4VP ratio. Electrochemical measurements indicate that the pores penetrate the methanol-rinsed films most deeply for those prepared using an initial DHN:4VP molar ratio of 4:1. It was estimated from these measurements that a P4VP layer of about 2 nm thick is located at the film−substrate interface, through which electron tunneling can occur.

Introduction

The achievement of regular nanoscopic functional patterns on various surfaces is a key issue for numerous applications including nanolithography, catalysis, data storage, optics, and nanoelectronics.[1−6] Block copolymers,[7] which have been widely studied in the bulk,[8] in solution,[9] and as thin films,[10,11] are well-known to self-assemble into meso- and nanoscale structures. A major challenge is obtaining and controlling long-range order and orientation of the nanostructured patterns. To achieve this in block copolymer thin films, various strategies have been developed. They range from chemical modification of the substrate surface in view of suitable substrate−polymer interactions, to the control of film thickness relative to the natural period of the polymer through the effect of boundary conditions, to the use of external fields including electric, crystallization, and solvent evaporation fields.[10]

Recently, a strategy that combines supramolecular chemistry with block copolymer self-assembly has been developed and provides a simple and powerful technique for controlling the formation of well-defined nanostructures in bulk[12−14] and in thin films.[15−17] In this approach, low molar mass substances are associated with one of the blocks by noncovalent interactions. Most frequently to date, small molecules bearing hydroxy and/or carboxylic acid functions have been hydrogen-bonded to pyridine functions in poly(styrene-*b*-4-vinylpyridine) (PS4VP) block copolymers. This results in an increase in the 4VP block fraction, thereby influencing the morphology obtained. In the bulk, this strategy was used with a long-chain alkyl phenol to fabricate a material with hierarchical morphology on two different length scales that was strongly amenable to thermal manipulation.[12] In dip-coated thin films of PS4VP [M_n(PS) = 35 500, M_n(P4VP) = 3680 g/mol], the use of a ditopic molecule with two different hydrogen-bonding groups, 2-(4′-hydroxyphenylazo)benzoic acid (HABA), was shown to give a cylindrical morphology where the cylinder axis can be oriented either horizontally or vertically (relative to the substrate) depending on the solvent used; this was related to the type of hydrogen bond (involving either the hydroxy or the acid group of HABA) favored in the presence of the solvent.[15]

A major advantage of the supramolecular strategy is that the low molar mass substance can be removed easily from the block copolymer nanopattern by selective dissolution to produce a nanoporous material with the same overall morphology as the parent material, shown in both the bulk[14,18] and the thin film materials[15] just described. It is noteworthy that the resulting nanopores are lined with functional groups that are available for further manipulation. As an example, it was demonstrated in ref 15 that the vertically oriented cylindrical nanoporous film could be used as a template to grow an ordered array of nickel nanodots via electrodeposition. In related work, Russell and coworkers have shown that thin poly(styrene-*b*-methyl methacrylate) (PS-*b*-PMMA) films with vertically oriented PMMA cylinders swelled by low molar mass PMMA also lead to (very small) pores after removal of the oligomer by selective dissolution.[19]

In this paper, we have applied the supramolecular approach described in ref 15 to thin films of a much higher molar mass PS4VP block copolymer [M_n(PS) = 71 900, M_n(P4VP) = 30 200 g/mol] where the relative fraction of the 4VP block is also much greater. It is complexed with a ditopic small molecule possessing a single type of hydrogen-bonding group, namely 1,5-dihydroxynaphthalene (DHN) (chosen in part for its low toxicity compared to phenol derivatives). The hydroxy groups are expected to hydrogen-bond to the VP groups, as illustrated in Figure 1. We show, in addition, that the DHN:VP stoichiometry is a useful parameter for controlling the geometric features of the thin film nanostructures achieved before and after the removal of DHN. The combination of AFM and TEM

* To whom correspondence should be addressed.
† Present address: NRC Industrial Materials Institute (NRC-IMI), 75 de Mortagne Blvd., Boucherville, QC, Canada J4B 6Y4.

10.1021/ma061129h CCC: $33.50
Published on Web 08/19/2006

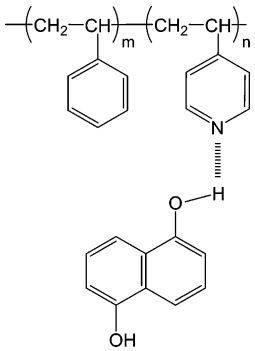

Figure 1. PS4VP + DHN supramolecular assembly.

techniques with readily available contact angle and cyclic voltammetry measurements together provide a good picture of various aspects of these films.

Experimental Section

Materials. The block copolymer poly(styrene-*b*-4-vinylpyridine) (PS4VP), with $M_n = 71\,900$ g/mol for PS and 30 200 g/mol for P4VP and $M_w/M_n = 1.08$ for PS and 1.13 for both blocks, was purchased from Polymer Source and used as received. 1,5-Dihydroxynaphthalene (DHN) (97%) was purchased from Aldrich, filtered in acetone using 0.45 μm PTFE filters, and recrystallized from acetone/hexane (50/50 v/v). Tetrahydrofuran (THF, 99.9%) and methanol (99.9%) were purchased from VWR and filtered twice with 0.2 μm PTFE filters before use.

Silicon wafers ({100}, 2 nm thick native oxide layer, as determined by ellipsometry), purchased from Wafer Works, were used as substrates unless otherwise specified. Several cleaning methods were tested with regards to the nanostructural order obtained after film deposition. It was concluded that simple rinsing in Millipore water, wiping with Kimwipe tissue, followed by rinsing in THF and drying under nitrogen flow provided surfaces clean enough to give the same results as obtained with stronger cleaning procedures such as ultrasonication in organic solvents followed by strong oxidative treatments like boiling "piranha" or "aqua regia" solutions. The simpler method was thus chosen for systematic cleaning of the silicon wafers just prior to film deposition.

Sample Preparation. To obtain the supramolecular assembly, the copolymer and DHN were dissolved together in THF at a constant copolymer concentration of 0.5 wt % and various DHN to copolymer ratios (specified as moles of DHN molecules relative to the VP moieties). The solutions were stirred at ca. 70 °C overnight in closed vials to ensure homogeneous mixing of the components. The block copolymer without DHN was similarly dissolved in THF and heated overnight at 40 °C. The solutions were filtered with 0.2 μm PTFE filters just before use. The substrates were dip-coated by vertically immersing the substrate into the solution at a rate of 10 mm/min, followed by a 20 s pause, and then raising the substrate out of the solution at a rate of 5 mm/min. The speeds were precisely controlled by using a KSV 3000 Langmuir film balance. The speed of immersion was not found to influence the order of the nanostructures (as long as the pause time was long enough to allow all perturbation to be fully damped), whereas faster pull-out speeds led to less ordered structures. The coated substrates were air-dried in Petri dishes. To remove the DHN, the coated substrates were immersed in methanol for 30 min and dried under nitrogen flow and then in a vacuum oven at 80 °C for 5 min to ensure complete methanol evaporation. The concentration of 0.5 wt % copolymer was found to give a film of uniform thickness over the entire surface of the substrate for equimolar DHN:4VP compositions. Higher concentrations or higher DHN:4VP molar ratios led to the partial deposition of a second layer on top of the first one (dewetting behavior); it has the same thickness as the first layer but shows a disordered nanostructured surface.

Fourier Transform Infrared Spectroscopy (FTIR). Infrared spectra were recorded with a Digilab Excalibur 3100 HE spectrometer equipped with a DGTS detector. The samples were solvent cast on sodium chloride pellets and dried overnight at 70 °C under dynamic vacuum. Spectra of the DHN-containing copolymer films were also taken after immersion into anhydrous methanol for 10 min, followed by drying at 70 °C under dynamic vacuum for 1 h.

Atomic Force Microscopy (AFM). AFM images were obtained in light tapping mode with a Multimode microscope and a Nanoscope III controller (Digital Instruments), operated under ambient atmosphere. The tips had spring constants between 1.5 and 3.7 $N.m^{-1}$ and oscillation frequencies between 170 and 350 Hz. The typical tip radius was below 10 nm. The experiments were repeated several times for each film composition, particularly frequently for the 1:1 and 4:1 (DHN:4VP molar ratio) samples, including for at least two separately prepared solutions from which the films were dip-coated. The geometric parameters reported are averages based on measurements obtained from several images for the same composition. To measure the film thickness, films deposited on silicon wafers were scratched with a scalpel, and AFM images were taken at the borders of the scratches; average values were obtained from several measurements along each of several scratches.

Transmission Electron Microscopy (TEM). TEM measurements were performed using a JEOL JEM 2000FX at 80 kV. Prior to film deposition, freshly cleaved mica substrates were carbon-coated (using a Cressington 108 Carbon/A vacuum carbon evaporator) to ease floating of the film at the water surface. (AFM experiments showed that the copolymer nanostructures were the same on silicon oxide, mica, and carbon substrates.) The films were then transferred onto copper grids using the floating technique. To enhance the contrast between the blocks, the samples were exposed to I_2 crystals for 24 h. Iodine vapor selectively stains the P4VP blocks and appears dark in the micrographs.

Cyclic Voltammetry (CV). Electrochemical measurements were performed using an Epsilon C3 potentiostat (Bioanalytical Systems) with the three-electrode configuration. The reference electrode was Ag/AgCl, NaCl (3 M) and the counter electrode a platinum foil. The electrolyte was a 5 mM $Fe(CN)_6^{3-}$/5 mM $Fe(CN)_6^{4-}$ ("ferri/ferrocyanide") aqueous solution, phosphate-buffered at pH 7 and 0.1 M NaCl. Millipore water (16.8 Ω·cm) was used, and the solution was filtered with a 0.45 μm PTFE filter just before use. Cyclic voltammograms were carried out from −0.3 to 0.7 V vs Ag/AgCl at various scan rates. Gold-coated glass slides (with an adhesion-enhancing interfacial chromium layer), graciously supplied by Dr. Ming Zhou of the National Research Council of Canada, Ottawa, were used as substrates. They were rinsed in THF and dried under nitrogen flow before film deposition. After film deposition, the area to be immersed in the electrolyte was delimited by epoxy resin. AFM imaging showed that adding a gold layer or electrochemical cycling in an aqueous solution did not modify the nanostructures obtained.

Contact Angle Measurements. Block copolymers and homopolymers were dip-coated from THF solutions onto silicon wafers. Millipore water drops (5 μL) were deposited on the surface, and the angle at the interface was measured. Images were taken using a First Ten Ångströms FTÅ200 apparatus. Contact angle data are average values of two opposite points of ca. 5 drops.

Results and Discussion

Supramolecular Assembly of PS4VP and DHN. It was first verified by FTIR that the two components PS4VP and DHN do indeed hydrogen-bond together. The spectra of DHN, PS4VP, and the equimolar DHN−PS4VP complex before and after DHN removal are shown in Figure 2. The free pyridine peaks at 993 and 1415 cm^{-1} (dotted lines) for PS4VP are shifted to 1008 and 1420 cm^{-1} (downward-pointing arrows), respectively, for the DHN−PS4VP complex. These shifts are clear evidence that the pyridine groups are hydrogen-bonded.[12b,d,15a,20] Furthermore, it can be concluded from the disappearance of the peak at 993 cm^{-1} that essentially all of the pyridines are hydrogen-bonded in the equimolar complex.

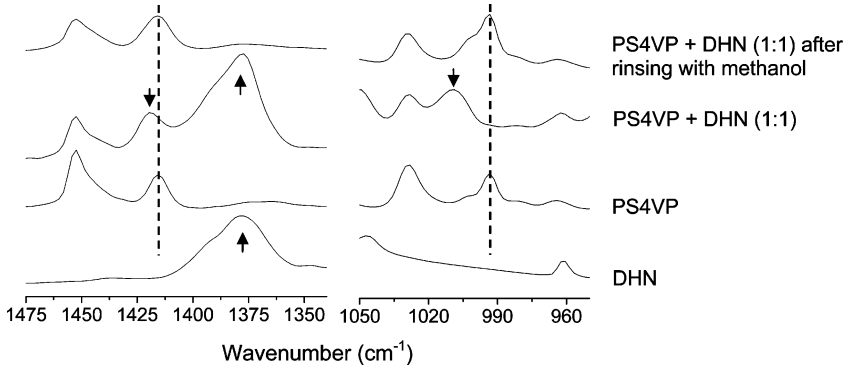

Figure 2. FTIR spectra of DHN, PS4VP, and the PS4VP + DHN complex (DHN:4VP molar ratio 1:1) before and after removal of DHN.

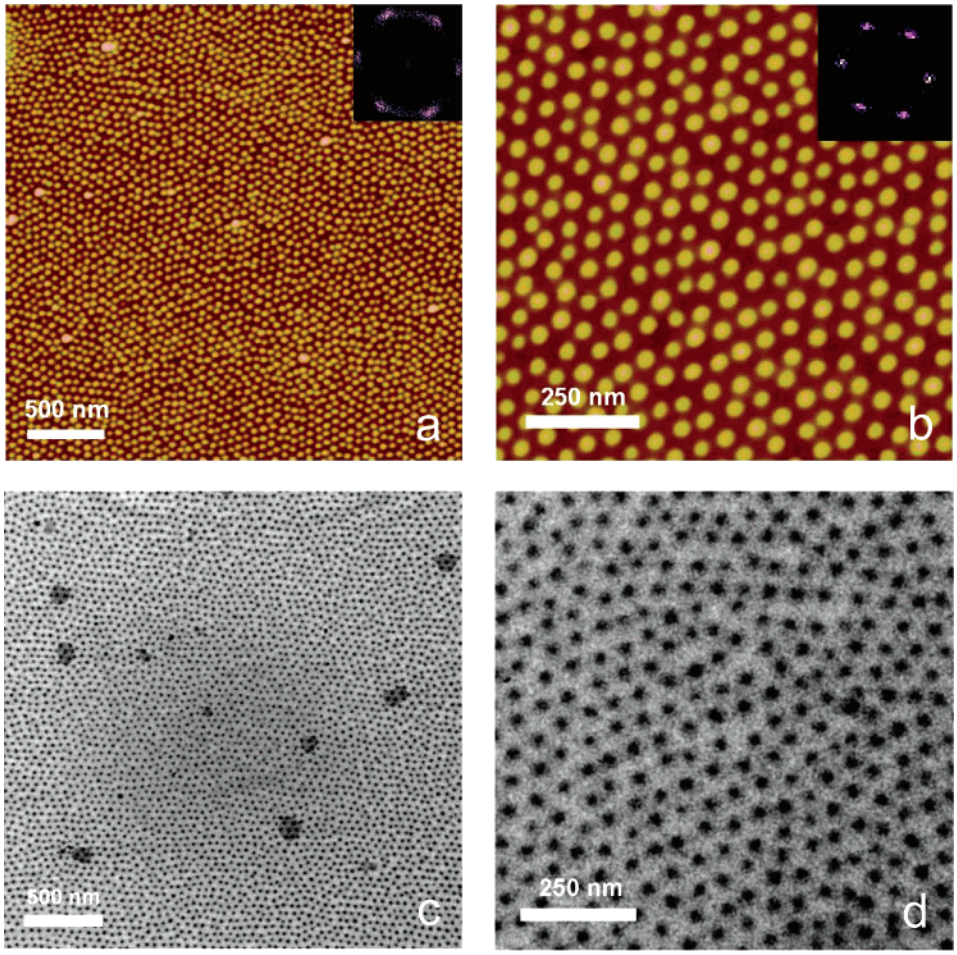

Figure 3. AFM height images (a, b) and TEM images (c, d) of a thin film of PS4VP + DHN (1:1 DHN:VP molar ratio) dip-coated on silicon. Fast Fourier transforms (FFT) of the AFM images are given in the insets of (a) and (b). AFM height scale: 0−20 nm. TEM films are I_2-stained.

After immersion of the film in methanol, the free pyridine peaks are recovered, whereas the characteristic DHN peaks have disappeared as shown in particular by the isolated DHN band at 1378 cm^{-1} (indicated in Figure 2 by the upward-pointing arrows). This demonstrates that rinsing with methanol is efficient for eliminating DHN from the copolymer, as was observed in ref 15 for HABA.

Film Morphology of the Equimolar Supramolecular Assembly. The copolymer used has a P4VP weight fraction of 0.3, which is just below the boundary composition of the cylindrical/lamellar morphological transition in the bulk.[12b] The selective addition of DHN to the P4VP phase induces an increase in the weight fraction of the latter, notably to 0.51 if the deposited film maintains the equimolar DHN:4VP composition of the solution, thus making the supramolecular assembly a symmetric copolymer system. It might therefore be expected that the deposited films also have a lamellar structure. However, the AFM and TEM images in Figure 3 show that a pattern of hexagonally ordered nodules in a continuous matrix is obtained. The AFM images indicate that the nodules protrude above the matrix. The TEM images reveal that the P4VP + DHN phase (dark dots) is located in the nodules and the PS phase (light regions) forms the matrix. This arrangement is qualitatively identical to that obtained for the PS4VP + HABA system of much lower P4VP weight fraction (0.10 and 0.25 before and after addition of equimolar HABA, respectively, the latter of which was shown to give a cylindrical morphology in the bulk) from a 1,4-dioxane solution.[15] It may be mentioned, in this

Table 1. Geometric Parameters of the Nanostructures in the Dip-Coated PS4VP Copolymer Films with and without DHN, before and after Rinsing with Methanol, As Measured from AFM (Normal Characters) and TEM (Bold Characters) Images[a]

DHN:4VP molar ratio	as-deposited				after immersion in methanol			
	ϕ_{nod}	d_{n-n}	h_{nod}	h_{film}	ϕ_{pore}	d_{p-p}	h_{pore}	h_{film}
no DHN	25 ± 5	45 ± 5	4 ± 1	15 ± 1	15 ± 5	47 ± 3	4 ± 2	14 ± 2
	27 ± 3	**47 ± 5**			**16 ± 4**	**48 ± 7**		
1:2	22 ± 13	40 ± 22	9 ± 2	*b*	13 ± 10	40 ± 15	7 ± 2	*b*
1:1	31 ± 3	48 ± 6	11 ± 2	7 ± 2	18 ± 3	47 ± 6	7 ± 1	7 ± 2
	25 ± 5	**50 ± 4**			**18 ± 4**	**45 ± 6**		
2:1	31 ± 6	51 ± 6	11 ± 2	9 ± 2	20 ± 3	47 ± 5	9 ± 1	11 ± 2
	20 ± 2	**56 ± 6**			*c*	**56 ± 11**		
4:1	31 ± 4	64 ± 6	7 ± 2	16 ± 2	25 ± 5	60 ± 5	18 ± 2	18 ± 2
	24 ± 3	**72 ± 11**			**26 ± 5**	**70 ± 10**		

[a] ϕ_{nod} = nodule diameter, d_{n-n} = center-to-center distance between nearest-neighbor nodules, h_{nod} = nodule protrusion above the matrix, h_{film} = film thickness at the matrix level, ϕ_{pore} = pore diameter, d_{p-p} = center-to-center distance between nearest-neighbor pores, and h_{pore} = pore depth. All data are in nm. The ranges given indicate minimum and maximum values measured. [b] Not measured. [c] Features not sufficiently regular to give reliable values.

connection, that we found the same pattern even for an initially nearly symmetric block copolymer for which the weight fraction of the P4VP phase becomes 0.7 after addition of equimolar DHN—that is, despite the P4VP + DHN being the apparent majority phase, it still leads, in films dip-coated from THF solutions, to a morphology of ordered P4VP + DHN nodules within a PS matrix.[21]

Similar behavior was observed for solution-cast films of styrene−butadiene di- and triblock copolymers with certain solvents.[22] This structure, where the minority block forms the continuum phase, was termed an "inverted phase", and it was attributed to the solvent—although good for both blocks—having a preferential affinity for the minority block. The consequence in a high concentration regime, which is the state of undried deposited films, is that this block is preferentially swollen with the solvent such that it is the effective majority phase; the resulting structure is frozen in upon sample drying.[22a] This may be compared to the case of symmetric block copolymers dissolved in solvents that are selective for one of the blocks, resulting in micellar solutions that can lead to an ordered micellar morphology in ultrathin films prepared from these solutions.[23,24] In our case, THF is a solvent for both blocks,[25] but with greater affinity for PS than for P4VP;[26,27] this may not be altered (or may be exacerbated) by complexation of P4VP with DHN. Other factors may contribute as well; in particular, the presence of DHN may affect interfacial interactions during the deposition and drying of the thin films (including possible effects of solvent evaporation rate[28−31]). Furthermore, it is not known whether the deposited film actually contains an equimolar amount of DHN.

The geometric parameters of the nanostructures viewed in the AFM and TEM images are summarized in Table 1. The film thickness is about 7 nm at the matrix level, with the nodules protruding about 11 nm higher to give a total thickness of nearly 20 nm. The protrusion of the P4VP + DHN nodules above the PS matrix is consistent with preferential swelling of the PS by THF in the deposited (undried) film, in that drying of such a film results in significant shrinkage of the matrix toward the substrate. Height differences ascribed to solvent preferences for one phase over the other have been reported for other copolymer and blend films.[26,27,32,33] The lateral order of the nanostructures is imperfect, but it clearly tends to organize in a two-dimensional hexagonal lattice, as shown by the fast Fourier transforms (FFT) of the AFM images (insets in Figure 2a,b). The average nodule diameter is about 30 nm and the average center-to-center distance between nearest-neighbor nodules about 50 nm. The diameters observed by AFM are somewhat larger than those observed by TEM, which might be caused by a significant amount of (covalently attached) PS embedding the nodules due to shrinkage of the adjacent swollen matrix around these objects during drying. It may also be due to an enlarging effect caused by the finite diameter of the AFM tips.[34]

Table 2. Water Contact Angles, θ (in deg), of the Dip-Coated PS4VP + DHN Copolymer Films at the DHN:4VP Molar Ratios Indicated, before and after Immersion into Methanol, and of the Corresponding Homopolymers

	PS	P4VP	DHN:4VP (1:1)	DHN:4VP (2:1)	DHN:4VP (4:1)
θ (as deposited film)	92 ± 3	62 ± 3	86 ± 4	86 ± 3	88 ± 4
θ (after MeOH rinse)			60 ± 5	62 ± 5	69 ± 3

Given that the maximum nodule height (equivalent to the total film thickness) is comparable to or even smaller than the nodule diameter, the morphology may be considered to be spherical in nature. On the other hand, the PS4VP + HABA system dip-coated from dioxane solution results in ordered P4VP + HABA domains that are significantly smaller in diameter (9.3 nm) than the film thickness (25−70 nm) and were concluded to be vertically oriented cylinders in a PS matrix.[15] From this point of view, and considering that the P4VP block in our case is much greater in weight fraction than for the copolymer used in ref 15, the nodules may also be considered to be perpendicularly oriented (short) cylinders.

It is of interest to note that, for our system, the use of THF gives exclusively nodular (spherical or perpendicularly oriented cylindrical) morphology, whereas the PS4VP + HABA system dip-coated from THF solution gives a mixture of horizontally and perpendicularly oriented cylinders.[15a] We verified that nodular morphology only was obtained also for the copolymer of identical composition as that in ref 15, which argues that it is the type of low molar mass additive that makes the difference and not the copolymer composition or molar mass. We are currently investigating this further with other hydrogen-bonding small molecules.

To probe the nature of the surface of the deposited film, the water contact angle was measured: Table 2 shows that it is close to that obtained for a PS homopolymer film. This indicates that most if not all of the film is covered by PS, including the nodules. This result is expected, since a PS surface layer minimizes the surface energy in air.[35] Tokarev et al.[15b] also measured a surface enrichment of the PS component (compared to the copolymer composition), using X-ray photoelectron spectroscopy, and concluded that a very thin layer of PS covers the entire sample of perpendicularly oriented cylinders.

Morphology of the Nanoporous Film. Rinsing the dip-coated film with methanol, which is a solvent for P4VP and DHN but not for PS, removes the DHN from the P4VP block,

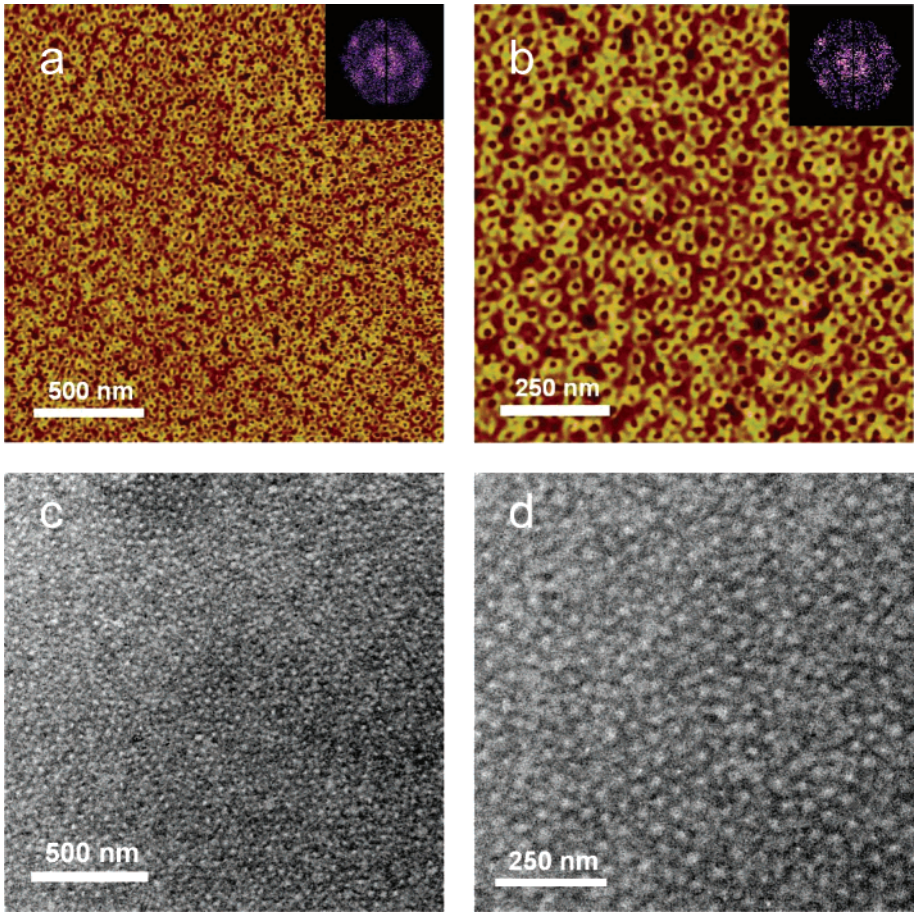

Figure 4. AFM height images (a, b) and TEM images (c, d) of the nanoporous film obtained after immersion of the dip-coated PS4VP + DHN thin film in methanol to remove DHN (initial DHN:4VP molar ratio 1:1). AFM height scale: 0−20 nm. TEM films are I_2-stained.

as demonstrated above by FTIR (Figure 2). The AFM images in Figure 4a,b show that this leads to a nanoporous film, qualitatively similar to that observed in ref 15 using the same procedure. Since the (solid) PS matrix is not swollen by methanol, it maintains the overall structure in place, whereas the decrease in volume fraction of the PS4VP + DHN phase after the removal of DHN and methanol leads to a shrinkage of the P4VP chains against the PS phase, thereby producing the P4VP-lined pores. On the surface of the film, these pores are surrounded by residual "lips" that protrude above the matrix level by about 3 nm, which is much less than the protrusion of the original nodules. As shown in Table 1, the nearest-neighbor center-to-center distance of the pores is essentially unchanged from that measured for the nodules before methanol rinsing. The average diameter measured for the pores is roughly two-thirds of that measured for the nodules, which is fairly close to what would be expected from the elimination of DHN (considering the respective molar volumes of DHN and VP). The film thickness at the matrix level appears unchanged compared to the film before methanol rinsing. Interestingly, the depth measured by AFM for the pores suggests that they penetrate the film thickness fully or almost fully. This point will be returned to in the last section.

The TEM images (Figure 4c,d), which show light dots distributed in a darker matrix, corroborate the porous nature of the film; the light dots in TEM are indicative of little or no (stained) material and correspond to the dark dots in AFM indicative of pores. The lightness of the dots is consistent with the pores penetrating the film deeply, in agreement with the AFM data. The average diameter and center-to-center distance of the pores also agree with the AFM measurements. The darkest tint is located at the periphery of the pores, consistent with their being lined with P4VP. It is notable that the matrix area is also distinctly gray, indicating the presence of P4VP there as well. From the water contact angle measured, which is the same as that for a P4VP homopolymer film (Table 2), it can be concluded that the entire surface is covered with P4VP. The fact that the film thickness appears unchanged before and after immersion into methanol indicates that the thickness of the P4VP surface layer is within the uncertainty of the film thickness measurements, that is, of the order of a nanometer or less. This rearrangement at the film surface could involve primarily the P4VP located in the nodular protrusions above the matrix in the parent film, thus accounting for the drastic reduction in the height of the "lips" after the methanol rinse. It is noted that surface rearrangement (also called reconstruction) of polymer films in response to environmental change is a well-known phenomenon.[26a,36−38]

The schematic representations shown in Figure 5 summarize the overall picture obtained for the dip-coated film of PS4VP + DHN (1:1) before and after the methanol rinse. What is not shown is the likelihood that there is a very thin P4VP layer wetting the entire film−substrate interface as well.[15] This will be addressed in the last section.

Film Morphology of PS4VP without DHN. For comparison, the morphology of PS4VP thin films without DHN was also investigated. An AFM height image of the PS4VP film dip-coated on a silicon substrate from a 1 wt % THF solution[39] is illustrated in Figure 6a. It shows a pattern similar to that obtained with DHN present, namely, nodules (presumably of P4VP) that

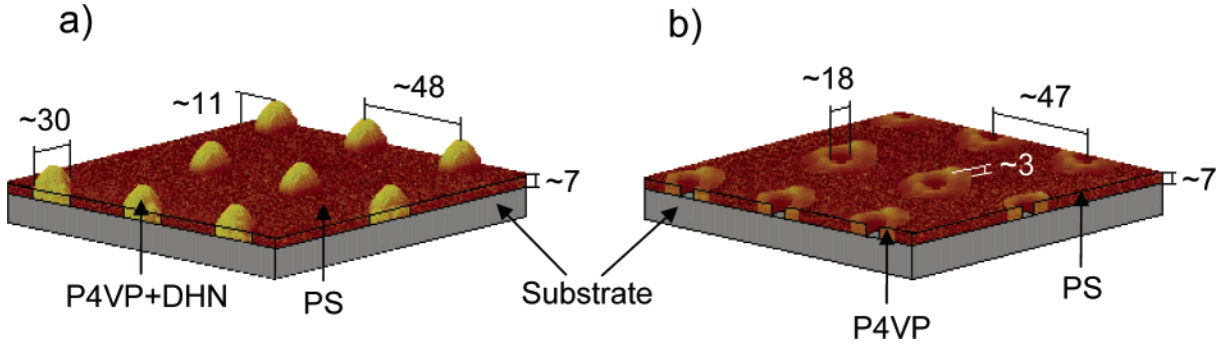

Figure 5. Schematic representations of the nanostructured PS4VP + DHN (1:1) film (a) as deposited and (b) after immersion in MeOH to eliminate DHN. All data are in nm. For clarity, the nanostructures have been laterally aerated. The PS covering the nodules in (a), the ultrathin layer of P4VP covering the PS matrix in (b), and an ultrathin P4VP wetting layer at the interface with the substrate are not shown.

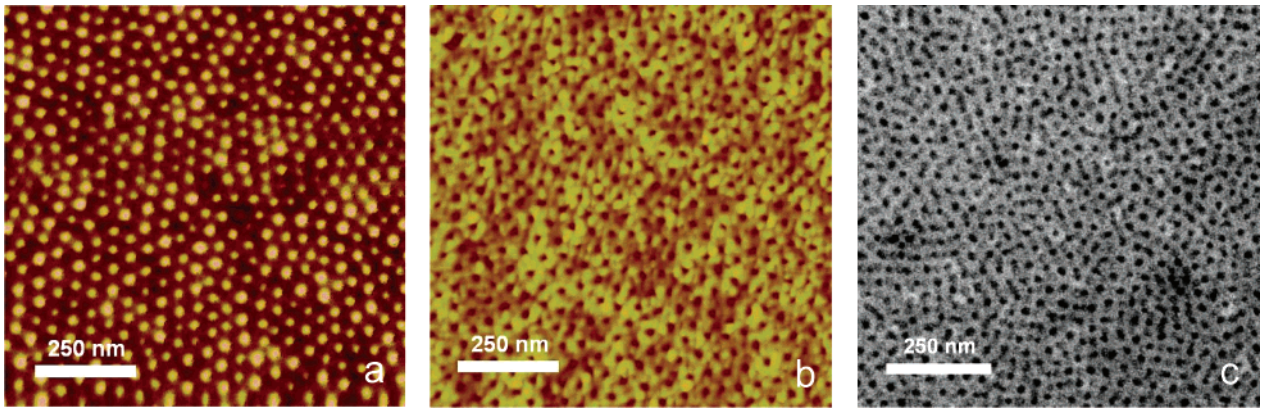

Figure 6. AFM height images (a, b) and TEM image (c) of a PS4VP thin film dip-coated on silicon from a 1 wt % solution before (a) and after (b, c) immersion in methanol. AFM height scale: 0−10 nm.

are arranged in a roughly hexagonal pattern with the same average periodicity. As shown in Table 1, the total film thickness (almost 20 nm) is the same as obtained for the film with DHN added; however, the thickness at the matrix level is doubled (about 15 nm), with a consequent reduction in the protrusion of the nodules (about 4 nm), for the film without DHN. A possible explanation is that the comparative swelling of PS by THF in the undried film is greater when DHN is present than when it is not, which suggests that hydrogen-bonding complexation of P4VP by DHN reduces the solubility of P4VP in THF, thus increasing the preference of THF for PS. Such an effect was also evoked in a note in ref 15b for 1,4-dioxane.

After immersion into methanol, the surface topography is modified, pores replacing the nodules in the same manner as for the films with DHN (Figure 6b). However, this time the pore depth as measured by AFM is only about 4 nm (Table 1). The shallowness of the pores is confirmed by the TEM image (Figure 6c), where the presence of the black dots (some of which appear interconnected) shows that the P4VP domains are still mainly located in nodules within a PS matrix. This indicates that the principal effect of methanol was to spread out the upper part of the P4VP nodules over the PS matrix (supported by the gray tint in most of the matrix area), leaving shallow depressions above the (partially eroded) nodules. A similar effect was observed for PS4VP copolymer thin films annealed under methanol vapor[40] or treated with water[41] and for films of PS-*b*-PMMA rinsed with PMMA-selective acetic acid.[42] In the latter case, the pores appeared to traverse the film thickness deeply, even completely; but this does not occur with the PS4VP films exposed to methanol or water (even after long times[40,41]), which contrasts with the behavior observed when a P4VP swelling agent like DHN or HABA is initially present.

Influence of the DHN:4VP Molar Ratio. Figure 7 shows the AFM height images of films deposited from solutions of different DHN:4VP ratios before and after DHN removal. The geometric parameters obtained from these images are summarized in Table 1.

At a DHN:4VP ratio of 1:2, the complex is stoichiometric with respect to the functional groups (OH:VP). The AFM images for this composition (Figure $7a_1$) show nodules that, compared to the 1:1 composition, are closer together, are smaller on average, have greater size dispersity (with some fused into larger domains), and appear to have greater lateral disorder. After DHN removal (Figure $7a_2$), they are replaced by pores, still with significant lateral disorder and variability in sizes and shapes, including some lateral channels. These observations suggest that more DHN is necessary to obtain well-ordered patterns. Given the bifunctionality of DHN, it is possible that this is related, at least in part, to a physical cross-linking phenomenon that is, in principle, present for DHN:VP molar ratios below 1:1.

At a molar ratio of 2:1, the DHN molecules are present in excess relative to the pyridine moieties. In deposited films, excess DHN may hydrogen-bond to DHN molecules that are directly hydrogen-bonded to P4VP, but it may also phase-separate. The large white areas on parts of the film surface in Figure $7b_1$ (also observed in TEM) are indicative of some phase separation. However, it did not interfere with the block copolymer deposition process, and as shown in Figure $7b_2$, a regular pore pattern is obtained after DHN removal (the phase-separated areas also being removed by methanol rinsing). The geometric dimensions of the nanostructures are similar to those obtained with the 1:1 ratio, with a small increase in the average pore diameter and depth and in film thickness. In addition, no lips around the pores are visible; instead, the pores seem to

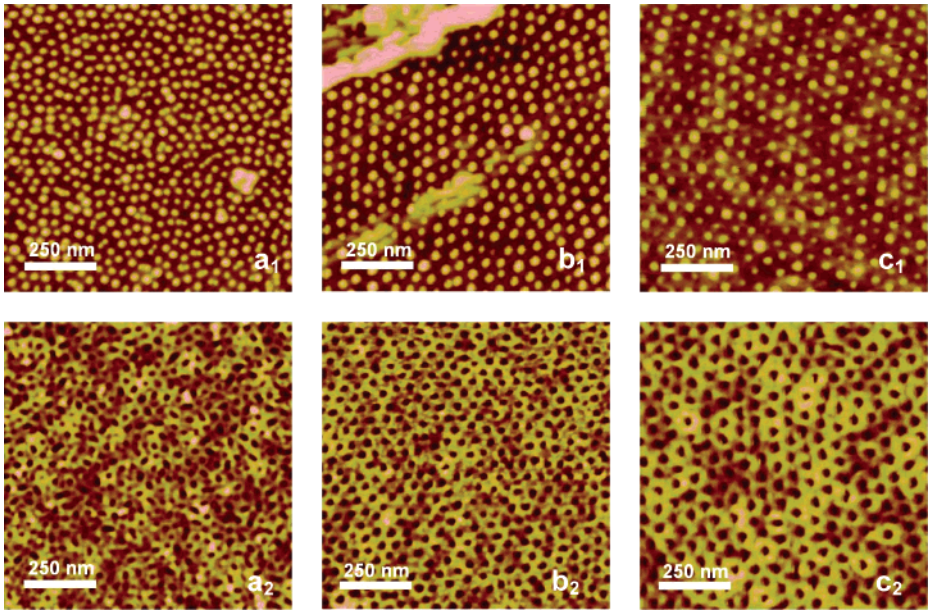

Figure 7. AFM height images of PS4VP + DHN thin films dip-coated on silicon, as deposited (subscript 1) and after DHN removal (subscript 2). DHN:4VP molar ratios: (a) 1:2, (b) 2:1, (c) 4:1. AFM height scale: 0−20 nm.

pierce a fairly homogeneous surface. Contact angle measurements are the same as obtained for the 1:1 ratio. These results suggest that, despite phase separation of a fraction of the DHN, a somewhat greater than stoichiometric amount of DHN was incorporated into the P4VP phase and had some influence on the structural parameters.

Much greater effects were obtained with the 4:1 molar ratio (Figure 7c and Table 1). In this case, we were able to obtain deposited films showing no DHN phase separation on the surface. This implies that it is possible to incorporate a large excess of DHN in the P4VP phase (although, again, it cannot be affirmed that the molar ratio in the deposited film is actually 4:1). Despite the still greater increase in weight fraction of the P4VP + DHN phase (up to 75% if all the DHN is incorporated), TEM imaging shows that the morphology of the deposited film remains in the form of P4VP + DHN nodules in a PS matrix. The periodicity of the nodules is significantly greater than for the other compositions, at about 70−80 nm (see Table 1). The film thickness at the matrix level is approximately doubled compared to the 1:1 and 2:1 ratios; however, the protrusion of the nodules is less, such that the total film thickness (at the nodule tops) is only moderately increased. The notable increase in the film thickness at the PS level with increase in DHN:4VP molar ratio above 1:1 suggests that the preference of THF for the PS phase is reduced by DHN in excess. Combining this with what was noted above for the 1:1 ratio and the copolymer with no DHN added, it appears that, whereas complexation of the P4VP block by DHN reduces the relative solubility of this block in THF, an excess of DHN beyond equimolar reverses this trend. An analogous effect is observed in aqueous solutions of polyelectrolytes with oppositely charged surfactants, where there is precipitation in the vicinity of stoichiometric compositions and resolubilization occurs as excess surfactant is added.[43]

After DHN removal, AFM images (Figure 7c_2) show the porelike surface morphology, which, by the absence of distinct lips around the pores, is similar to that for the 2:1 ratio. The corresponding TEM images (Figure 8) are particularly impressive. The white pores (indicating very little or no stained material) are very well-defined and are clearly delimited by a dark ring (indicating the location of stained P4VP). Thus, the P4VP phase appears to be strongly concentrated around the pores. The uneven gray-to-whitish color of the matrix suggests that the surface may not be completely covered by a P4VP layer. This is supported by the water contact angle measured for this surface (near 70°, Table 2), indicating that a fraction of the PS remains exposed. The pore diameter is much greater than for the 1:1 molar ratio, as would be expected from the elimination of a much greater amount of DHN, and the pore depth appears to match the film thickness, suggesting complete or almost complete penetration of the film (despite its much greater thickness compared to the lower molar ratios). Surprisingly, the average pore diameter appears to be essentially the same as the average nodule diameter before DHN removal (and the latter is the same as that for the 1:1 molar ratio), an observation which is not understood at this time.

It may be added that attempts to prepare similar films using an 8:1 DHN/4VP ratio were unsuccessful. In this case, phase-separated DHN appeared to interfere with the deposition process, and ordered nanostructures were not obtained.

Evaluation of Pore Penetration of the Film Using Cyclic Voltammetry. When comparing films thicknesses measured using the scalpel technique and pores depths measured by AFM, the uncertainties in the measurements are too large to conclude definitively whether the pores penetrate the film completely. In this context, one is reminded that successful electrochemical growth of nickel in the pores of a similar nanoporous membrane was reported in ref 15a, whereas X-ray reflectivity analysis indicated that a layer of ca. 1.5 nm of P4VP remains at the bottom of the pores.[15b] These two facts might seem contradictory. To help clarify this aspect, we performed electrochemical experiments.

Films were deposited on a gold substrate, and the electroactivity of ferri/ferrocyanide salts ($Fe(CN)_6^{3-}/Fe(CN)_6^{4-}$) was probed using cyclic voltammetry. Figure 9 shows the oxidation/reduction peaks of the ferri/ferrocyanide on contact with the gold electrode before and after film deposition and after immersion into methanol. The shape of the peaks on a bare gold surface is well-known. The intensity of the signal is proportional to the quantity of molecules that undergo oxidation/reduction, and the difference between the peak potentials is

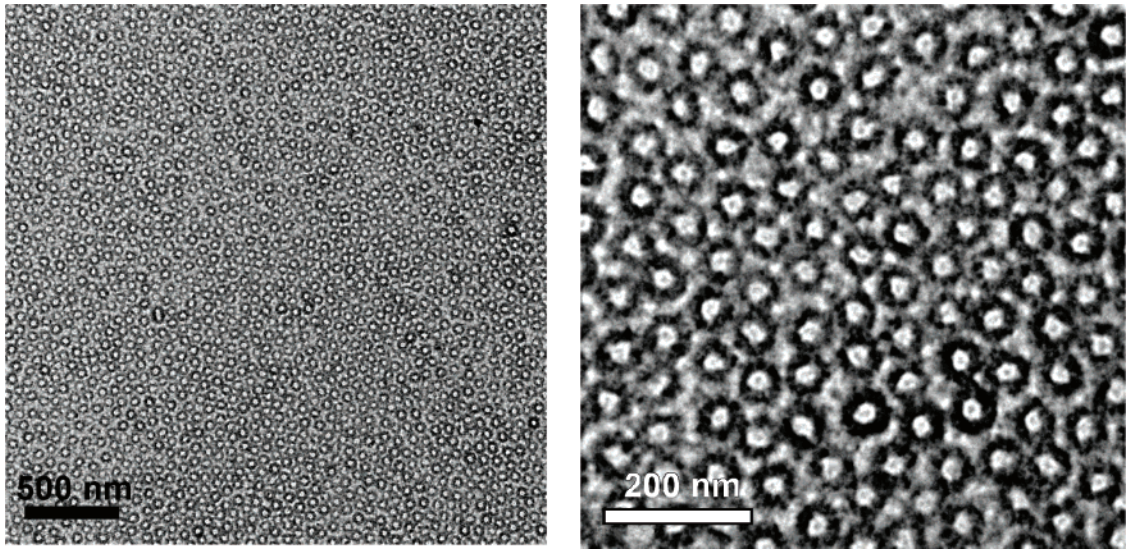

Figure 8. TEM images of the I_2-stained nanoporous film obtained by immersion of the dip-coated PS4VP + DHN thin film (DHN:4VP molar ratio 4:1) in methanol to remove DHN.

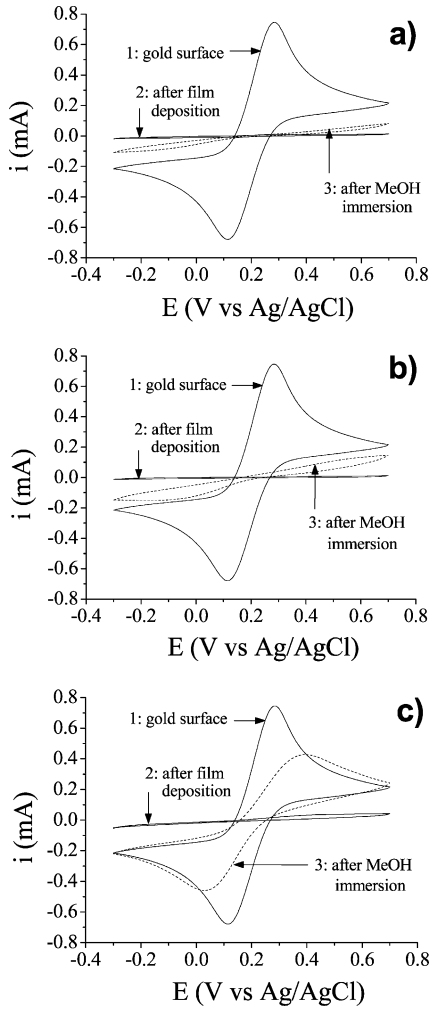

Figure 9. Cyclic voltammograms of $Fe(CN)_6^{3-}/Fe(CN)_6^{4-}$ on gold substrates (1) before and (2) after coating with a PS4VP + DHN thin film and (3) after removal of DHN by immersion in methanol. DHN:4VP molar ratios: (a) 1:1, (b) 2:1, (c) 4:1.

related to the kinetics of the electrochemical process. After film deposition, the electrochemical signal almost disappears, independently of the DHN:4VP ratio. This indicates that the copolymer film acts as a physical barrier that prevents the ferri/ferrocyanide molecules from reaching the gold surface as well as an electrical barrier that prevents electrons from passing through.

After immersion of the film into methanol and consequent pore formation, the electrochemical behavior depends on the DHN:4VP ratio. For a 1:1 ratio (Figure 9a), the signal is just slightly increased, revealing that the film stills acts as a barrier. This indicates that the pores observed by AFM do not actually reach the substrate. For a 2:1 ratio (Figure 9b), the intensity is increased a little, but the signal is still very weak compared to the gold surface. For a 4:1 ratio, however, significant electrochemical activity is observed, indicating that many ferri/ferrocyanide molecules are able to undergo oxidation/reduction reactions (Figure 9c). It should be noted that the intensity of the signal cannot reach the values observed with the bare electrode because a film is still present at the surface so that only a fraction of the total gold area is available for reaction.

Although electrochemical activity on the porous 4:1 film is clearly present, it can also be observed (Figure 9c) that the potential difference between the oxidation and reduction peaks after pore formation is greater than that on the bare gold surface. This implies that the electrochemical process must overcome an ohmic barrier (the oxidation occurs at a higher potential and the reduction at a more reductive potential). This phenomenon can be caused by two processes: a limitation due to the diffusion of the electroactive species into the pores of the film or the presence of an ultrathin layer of copolymer at the bottom of the pores through which electrons can migrate by a tunneling process.[44−46] Since the copolymer blocks are largely composed of aromatic rings, the tunneling of electrons through the π-orbitals should be possible if the thickness does not exceed a few nanometers.

The first process (a limitation due to diffusion) was tested by a kinetic experiment. To this end, cyclic voltammograms were taken at various scan rates (Figure 10), and the peak intensities were plotted as a function of the square root of the scan rate (inset of Figure 10). A normal linear relationship is obtained for the latter, which shows that the electrochemical process is limited only by the usual diffusion of the electroactive species in solution in the proximity of the electrode.[47] This excludes a limitation due to a slower diffusion of the molecules into the pores.

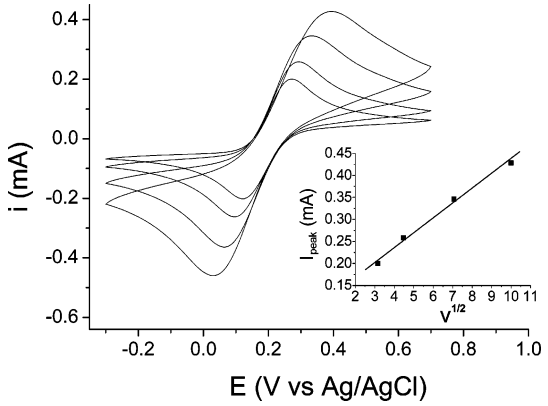

Figure 10. Cyclic voltammograms at different scan rates (5, 10, 20, and 100 mV/s) of $Fe(CN)_6^{3-}/Fe(CN)_6^{4-}$ on gold substrates after coating with a PS4VP + DHN thin film and subsequent removal of DHN with methanol (DHN:4VP molar ratio 4:1). The inset shows the linear relationship between the peak intensity (I_{peak}) and the square root of the scan rate (υ).

The presence of an ultrathin copolymer layer at the bottom of the pores, presumably of polar P4VP that wets the polar substrate, is thus the more probable explanation for the slowing down of electrochemical process. In this case, a tunneling process must occur to permit electrochemical activity. The credibility of this hypothesis was tested by using the electrochemical data to estimate the thickness of polymer film traversed by the electrons according to the kinetics of electron tunneling. This is described by the following equation

$$k_{app}^0 = k^0 e^{-\beta d} \quad (1)$$

where k_{app}^0 is the apparent heterogeneous rate constant, k^0 the heterogeneous rate constant on the free surface, β the tunneling parameter, and d the tunneling distance (i.e., the layer thickness).[44−46] The rate constants were calculated from the potential difference between the anodic and cathodic peaks in Figure 9c following Nicholson's method[48] and are 0.008 and 0.1 cm/s for the covered and free surface, respectively. The term β depends on the tunneling mechanism and hence on the nature of the layer and has been estimated to be between 1 and 2 nm^{-1} for unsaturated polyene layers.[44−46] Using these values in eq 1, the copolymer present at the bottom of the pores is estimated to be between 1.3 and 2.5 nm. This estimation is in excellent agreement with the thickness of the wetting layer determined by Tokarev et al. from X-ray reflectivity (1.5 nm),[15b] thus supporting the tunneling mechanism. This mechanism also explains why it is possible to electrochemically grow nickel in the pores despite the presence of the wetting layer at the substrate, as observed in ref 15.

Conclusions

The work presented here follows up on the supramolecular approach introduced by Stamm and colleagues for fabricating nanopatterned and nanoporous diblock films on surfaces, using low molar mass molecules that specifically associate with one of the blocks.[15] They illustrated this approach using a fairly low molar mass asymmetric PS4VP diblock copolymer (about 40 000 g/mol and 10% VP) and a ditopic small molecule (HABA) that hydrogen bonds to the VP through either the hydroxyl or carboxylic acid group of HABA, resulting in a cylindrical morphology that is horizontally and perpendicularly aligned to the surface, respectively, depending on the solvent used (chloroform and 1,4-dioxane, respectively). Subsequently, the HABA can be washed out with a selective solvent, leaving a nanoporous material in the case of the film with the vertical cylindrical morphology. The vertical cylinders and pores are ordered in a quasi-hexagonal pattern. In the present contribution, it is shown that a much higher molar mass and less asymmetric PS4VP block copolymer (about 100 000 g/mol and 30 wt % VP) similarly leads to a quasi-hexagonal nodular morphology of enriched P4VP in a PS matrix, this time using a ditopic molecule (DHN) with a single type of hydrogen-bonding function (hydroxyl). This was obtained in THF (tested also with other PS4VP compositions), a solvent that, for the system of Stamm and colleagues, resulted in a mixed morphology of vertical and horizontal cylinders. This seems to indicate that the choice of small molecule, in addition to the solvent, is an important factor in determining the morphology of the deposited film.

To rationalize the nodular morphology obtained in the PS4VP + DHN system (which, given its composition, is expected to give a lamellar morphology in the bulk—in contrast to the more asymmetric PS4VP + HABA system of Stamm and colleagues, which was determined to give a cylindrical morphology in the bulk), as well as the trends in some geometric parameters of the deposited films as a function of DHN content (including no DHN), the preferential solubility of PS over P4VP in THF was considered. Preferential solubility can lead to greater swelling of the PS phase, such that cylindrical or even spherical morphology is preferred in the undried film deposited, which is then frozen in on drying. This is supported by the fact that the P4VP + DHN nodules protrude above the matrix phase and by similar phenomena for other systems reported in the literature (see above). From this point of view, the trends in the nodule−matrix height difference and in the film thickness at the matrix level as a function of 4VP:DHN molar ratio suggest that the greatest difference in the solubilities of the two blocks in THF occurs for the equimolar 4VP:DHN ratio.

After extraction of the DHN by immersion in methanol, nanoporous films are obtained just as for the system of Stamm and colleagues. In addition, we show that the diameter and depth of penetration of the pores can be strongly influenced by the DHN content. This was particularly evident by comparing the films obtained from solutions containing no DHN, equimolar DHN, and 4× equimolar DHN. With no DHN present, the pores are shallow, whereas they appear to penetrate the film deeply when DHN is used, according to AFM and TEM images. On the other hand, cyclic voltammetry measurements showed that only the nanoporous film formed from the 4× equimolar DHN solution (the highest composition for which good films were obtained) gives a strong electrochemical signal. Furthermore, this quite simple technique allowed an estimation to be made of thickness of the wetting layer remaining at the bottom of the pores (ca. 2 nm), which agrees very well with what was determined by Stamm and colleagues using X-ray reflectivity. Since this estimation is based on a tunneling process, it simultaneously rationalizes the ability to electrochemically grow metal in the pores.

Finally, water contact angle measurements were useful in determining the nature of the surface of the films before and after methanol rinsing. Thus, a set of quite easily available techniques allowed us to obtain a good overall picture of the system under study.

Acknowledgment. Funding by the Advanced Food and Materials Network of Canada (AFMNet), a Canadian Center of Excellence, as well as NSERC Canada, is gratefully acknowl-

CDV

edged. The authors are members of the Centre for Self-Assembled Chemical Structures (CSACS), a Quebec FQRNT-funded Center of Excellence. Dr. H. Vali of McGill University is thanked for use of the TEM facility (FEMR). A. Laforgue thanks Prof. Thomas P. Russell and Dr. Du Yeol Ryu of the University of Massachussetts, Amherst, for their hospitality and useful discussions during a training visit.

References and Notes

(1) Hamley, I. W. *Nanotechnology* **2003**, *14*, R39.
(2) Park, C.; Yoon, J.; Thomas, E. L. *Polymer* **2003**, *44*, 6725.
(3) Lazzari, M.; López-Quintela, M. A. *Adv. Mater.* **2003**, *15*, 1583.
(4) Mendes, P. M.; Preece, J. A. *Curr. Opin. Colloid Interface Sci.* **2004**, *9*, 236.
(5) Glass, R.; Möller, M.; Spatz, J. P. *Nanotechnology* **2003**, *14*, 1153. Glass, R.; Arnold, M.; Cavalcanti-Adam, E. A.; Blümmel, J.; Haferkemper, C.; Dodd, C.; Spatz, J. P. *New J. Phys.* **2004**, *6*, 101.
(6) Krausch, G.; Magerle, R. *Adv. Mater.* **2002**, *14*, 1579.
(7) Hamley, I. W. *The Physics of Block Copolymers*; Oxford University Press: Oxford, 1998.
(8) Abetz, V.; Simon, P. F. W. *Adv. Polym. Sci.* **2005**, *189*, 125.
(9) Gohy, J.-F. *Adv. Polym. Sci.* **2005**, *190*, 65.
(10) Li, M.; Coenjarts, C.; Ober, C. K. *Adv. Polym. Sci.* **2005**, *190*, 183.
(11) Green, P. F.; Limary, R. *Adv. Colloid Interface Sci.* **2001**, *94*, 53.
(12) (a) Ruokolainen, J.; Mäkinen, R.; Torkkeli, M.; Mäkelä, T.; Serimaa, R.; ten Brinke, G.; Ikkala, O. *Science* **1998**, *280*, 557. (b) Ruokolainen, J.; Saariaho, M.; Ikkala, O.; ten Brinke, G.; Thomas, E. L.; Torkkeli, M.; Serimaa, R. *Macromolecules* **1999**, *32*, 1152. (c) Ruokolainen, J.; ten Brinke, G.; Ikkala, O. *Adv. Mater.* **1999**, *11*, 777. (d) Bondzic, S.; de Wit, J.; Polushkin, E.; Schouten, A. J.; ten Brinke, G.; Ruokolainen, J.; Ikkala, O.; Dolbnya, I.; Bras, W. *Macromolecules* **2004**, *37*, 9517.
(13) Hong, J.-Y.; Hong, J.-L. *J. Polym. Res.* **2004**, *11*, 89.
(14) (a) Fahmi, A. W.; Braun, H.-G.; Stamm, M. *Adv. Mater.* **2003**, *15*, 1201. (b) Fahmi, A. W.; Brünig, H.; Weidisch, R.; Stamm, M. *Macromol. Mater. Eng.* **2005**, *290*, 136. (c) Fahmi, A. W.; Stamm, M. *Langmuir* **2005**, *21*, 1062.
(15) (a) Sidorenko, A.; Tokarev, I.; Minko, S.; Stamm, M. *J. Am. Chem. Soc.* **2003**, *125*, 12211. (b) Tokarev, I.; Krenek, R.; Burkov, Y.; Schmeisser, D.; Sidorenko, A.; Minko, S.; Stamm, M. *Macromolecules* **2005**, *38*, 507.
(16) Liang, C.; Hong, K.; Guiochon, G. A.; Mays, J. W.; Dai, S. *Angew. Chem.* **2004**, *116*, 5909.
(17) Lu, Q.; Bazuin, C. G. *Nano Lett.* **2005**, *5*, 1309.
(18) (a) Mäki-Ontto, R.; de Moel, K.; de Odorico, W.; Ruokolainen, J.; Stamm, M.; ten Brinke, G.; Ikkala, O. *Adv. Mater.* **2001**, *13*, 117. (b) Ikkala, O.; ten Brinke, G. *Science* **2002**, *295*, 2407.
(19) (a) Jeong, U.; Kim, H.-C.; Rodriguez, R. L.; Tsai, I. Y.; Stafford, C. M.; Kim, J. K.; Hawker, C. J.; Russell, T. P. *Adv. Mater.* **2002**, *14*, 274. (b) Jeong, U.; Ryu, D. Y.; Kim, J. K.; Kim, D. H.; Wu, X.; Russell, T. P. *Macromolecules* **2003**, *36*, 10126. (c) Jeong, U.; Ryu, D. Y.; Kim, J. K.; Kim, D. H.; Russell, T. P.; Hawker, C. J. *Adv. Mater.* **2003**, *15*, 1247.
(20) Eichhorn, K.-J.; Fahmi, A.; Adam, G.; Stamm, M. *J. Mol. Struct.* **2003**, *661*−*662*, 161.
(21) Laforgue, A.; Bazuin, C. G.; Prud'homme, R. E. Unpublished results.
(22) (a) Huang, H.; Hu, Z.; Chen, Y.; Zhang, F.; Gong, Y.; He, T.; Wu, C. *Macromolecules* **2004**, *37*, 6523. (b) Huang, H.; Zhang, F.; Hu, Z.; Du, B.; He, T.; Lee, F. K.; Wang, Y.; Tsui, O. K. C. *Macromolecules* **2003**, *36*, 4084. (c) Zhang, Q. L.; Tsui, O. K. C.; Du, B.; Zhang, F. J.; Tang, T.; He, T. B. *Macromolecules* **2000**, *33*, 9561.
(23) (a) Meiners, J. C.; Ritzi, A.; Rafailovich, M. H.; Sokolov, J.; Mlynek, J.; Krausch, G. *Appl. Phys. A* **1995**, *61*, 519. (b) Meiners, J. C.; Elbs, H.; Ritzi, A.; Mlynek, J. Krausch, G. *J. Appl. Phys.* **1996**, *80*, 2224. (c) Meiners, J. C.; Quintel-Ritzi, A.; Mlynek, J.; Elbs, H.; Krausch, G. *Macromolecules* **1997**, *30*, 4945.
(24) Xuan, Y.; Peng, J.; Cui, L.; Wang, H.; Li, B.; Han, Y. *Macromolecules* **2004**, *37*, 7301.
(25) Brandrup, J., Immergut, E. H., Grulke, E. A., Eds. *Polymer Handbook*, 4th ed.; Wiley: New York, 1999.
(26) (a) Elbs, H.; Fukunaga, K.; Stadler, R.; Sauer, G.; Magerle, R.; Krausch, G. *Macromolecules* **1999**, *32*, 1204. (b) Böltau, M.; Walheim, S.; Mlynek, J.; Krausch, G.; Steiner, U. *Nature (London)* **1998**, *391*, 877.
(27) Cui, L.; Peng, J.; Ding, Y.; Li, X.; Han, Y. *Polymer* **2005**, *46*, 5334.
(28) Turturro, A.; Gattiglia, E.; Vacca, P.; Viola, G. T. *Polymer* **1995**, *36*, 3987.
(29) Kim, G.; Libera, M. *Macromolecules* **1998**, *31*, 2569.
(30) Kim, S. H.; Misner, M. J.; Xu, T.; Kimura, M.; Russell, T. P. *Adv. Mater.* **2004**, *16*, 226.
(31) Elbs, H.; Drummer, C.; Abetz, V.; Krausch, G. *Macromolecules* **2002**, *35*, 5570.
(32) Tanaka, K.; Takahara, A.; Kajiyama, T. *Macromolecules* **1996**, *29*, 3232.
(33) (a) Walheim, S.; Böltau, M.; Mlynek, J.; Krausch, G.; Steiner, U. *Macromolecules* **1997**, *30*, 4995. (b) Böker, A.; Müller, A.; Krausch, G. *Macromolecules* **2001**, *34*, 7477.
(34) Xu, S.; Arnsdorf, M. F. *J. Microsc.* **1997**, *187*, 43.
(35) (a) Green, P. F.; Christensen, T. M.; Russell, T. P.; Jérôme, R. *Macromolecules* **1989**, *22*, 2189. (b) Huang, E.; Mansky, P.; Russell, T. P.; Harrison, C.; Chaikin, P. M.; Register, R. A.; Hawker, C. J.; Mays, J. *Macromolecules* **2000**, *33*, 80.
(36) Andrade, J. D. In *Polymer Surface Dynamics*; Andrade, J. D., Ed.; Plenum Press: New York, 1988; Chapter 1.
(37) (a) Mori, H.; Hirao, A.; Nakahama, S.; Senshu, K. *Macromolecules* **1994**, *27*, 4093. (b) Senshu, K.; Yamashita, S.; Mori, H.; Ito, M.; Hirao, A.; Nakahama, S. *Langmuir* **1999**, *15*, 1754.
(38) Rehse, N.; Knoll, A.; Magerle, R.; Krausch, G. *Macromolecules* **2003**, *36*, 3261.
(39) The solution concentration was increased compared to that used for the DHN-containing solutions because it was found that PS−P4VP films dip-coated from a 0.5 wt % solution show incommensurability effects. As indicated by AFM and TEM images before and after rinsing with methanol, the latter films were composed of isolated regions showing the quasi-hexagonally ordered nodule morphology (total thickness of ca. 19 nm) surrounded by thinner regions (ca. 8 nm). Before rinsing with MeOH, these thinner regions are covered by a PS layer (unstained by I_2). After immersion in MeOH, they show a wormlike morphology ascribed to alternating PS and P4VP domains. In parallel, the water contact angle decreases from ca. 91° to 80° following rinsing; interestingly, the latter roughly matches what would be expected from the relative fractions of the two blocks (about 2/3 PS and 1/3 P4VP).
(40) Zhao, J.; Jiang, S.; Ji, X.; An, L.; Jiang, B. *Polymer* **2005**, *46*, 6513.
(41) Cong, Y.; Zhang, Z.; Fu, J.; Li, J.; Han, Y. *Polymer* **2005**, *46*, 5377.
(42) Xu, T.; Stevens, J.; Villa, J.; Goldbach, J. T.; Guarini, K. W.; Black, C. T.; Hawker, C. J.; Russell, T. P. *Adv. Funct. Mater.* **2003**, *13*, 698.
(43) Goddard, E. D. In *Interactions of Surfactants with Polymers and Proteins*; Goddard, E. D., Ananthapadmanabhan, K. P., Eds.; CRC Press: Boca Raton, FL, 1993; Chapter 4, p 177.
(44) Kariuki, J. K.; McDermott, M. T. *Langmuir* **2001**, *17*, 5947.
(45) Yang, H.-H.; McCreery, R. L. *Anal. Chem.* **1999**, *71*, 4081.
(46) Laforgue, A.; Addou, T.; Bélanger, D. *Langmuir* **2005**, *21*, 6855.
(47) Bard, A. J.; Faulkner, L. R. *Electrochemical Methods: Fundamentals and Applications*, 2nd ed.; John Wiley & Sons: New York, 2001.
(48) Nicholson, R. S. *Anal. Chem.* **1965**, *37*, 1351.

MA061129H